Title: **Plastic Deformation Capacity of Steel Beam-to-Column Connection under Long-duration Earthquake**

Authors: Satoshi Yamada, Tokyo Institute of Technology
Yu Jiao, Tokyo University of Science
Hiroyuki Narihara, Taisei Corporation
Satoshi Yasuda, Taisei Corporation
Takashi Haesgawa, Building Research Institute

Subject: Seismic

Keyword: Seismic

Publication Date: 2014

Original Publication: International Journal of High-Rise Buildings Volume 3 Number 3

Paper Type:
1. Book chapter/Part chapter
2. **Journal paper**
3. Conference proceeding
4. Unpublished conference paper
5. Magazine article
6. Unpublished

International Journal of High-Rise Buildings
September 2014, Vol 3, No 3, 231-241

International Journal of
High-Rise Buildings
www.ctbuh-korea.org/ijhrb/index.php

Plastic Deformation Capacity of Steel Beam-to-Column Connection under Long-duration Earthquake

Satoshi Yamada[1,†], Yu Jiao[2], Hiroyuki Narihara[3], Satoshi Yasuda[3], and Takashi Hasegawa[4]

[1]*Structural Engineering Research Center, Tokyo Institute of Technology, Yokohama 226-8503, Japan*
[2]*Faculty of Engineering, Tokyo University of Science, Tokyo 125-0051, Japan*
[3]*Technology Center, Taisei Corporation, Yokohama 245-0051, Japan*
[4]*Building Research Institute of Japan, Tsukuba 305-0802, Japan*

Abstract

Ductile fracture is one of the most common failure modes of steel beam-to-column connections in moment resisting frames. Most proposed evaluation methods of the plastic deformation capacity of a beam until ductile fracture are based on steel beam tests, where the material's yield strength/ratio, the beam's moment gradient, and loading history are the most important parameters. It is impossible and unpractical to cover all these parameters in real tests. Therefore, a new attempt to evaluate a beam's plastic deformation capacity through analysis is introduced in this paper. Another important issue is about the loading histories. Recent years, the effect on the structural component under long-duration ground motion has drawn great attentions. Steel beams tends to experience a large number of loading cycles with small amplitudes during long-duration earthquakes. However, current research often focuses on the beam's behavior under standard incremental loading protocols recommended by respective countries. In this paper, the plastic deformation capacity of steel beams subjected to long duration ground motions was evaluated through analytical methodology.

Keywords: Beam-to-column connection, Ductile fracture, In-plane analysis, Cyclic loading tests, Plastic deformation capacity, Long-duration earthquake

1. Introduction

In the 1994 Northridge earthquake and the 1995 Kobe earthquake, a great number of steel beam damage caused by brittle fracture was observed (Youssef et al., 1995). After that, many efforts have been made to prevent the brittle fracture of the beam under large amplitude cyclic loading (Nakashima et al., 1998; Roeder, 2002). Consequently, the loading protocols commonly employed in the beam tests are some standard recommended loading protocols such as the SAC protocol (Clark et al., 1997) in the U.S. and the JISF protocol (Building Research Institute and the Japan Iron and Steel Federation, 2002) recommended by the Building Research Institute and the Japan Iron and Steel Federation (Fig. 1). Most of these recommended loading protocols are incremental amplitude cyclic loadings.

Earthquake ground motions tend to have longer durations and long-period characteristics when the magnitude scale of the earthquake is large. During the 2011 Great Tohoku Earthquake, many high-rise buildings in Tokyo and Osaka, which are far away from the epicenter, also experienced long period of shaking, although no damage was reported. The ground motion acceleration time histories of the Kobe earthquake (near-fault, Mw 6.9) and the Tohoku earthquake (Off-shore, Mw 9.0) are shown in Fig. 2. In these graphs, JMA Kobe was recorded at the site 24.8 km from the epicenter (JMA SGM database), while

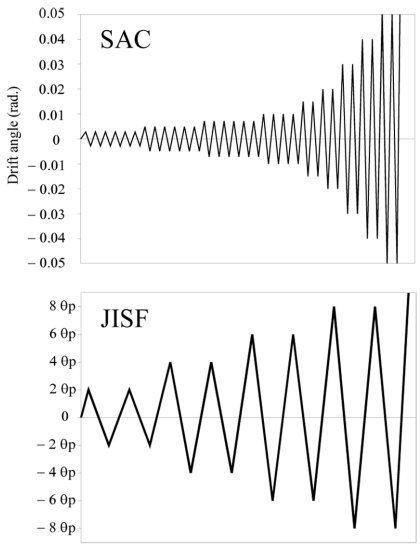

Figure 1. Typical recommended loading protocols.

†Corresponding author: Satoshi Yamada
Tel: +81-45-924-5330; Fax: +81-45-924-5334
E-mail: yamada.s.ad@m.titech.ac.jp

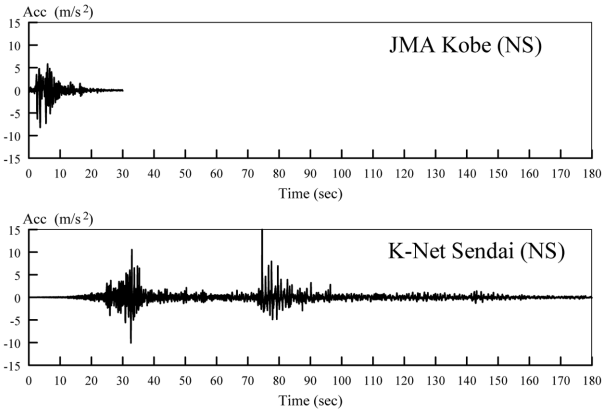

Figure 2. Ground motion acceleration time histories.

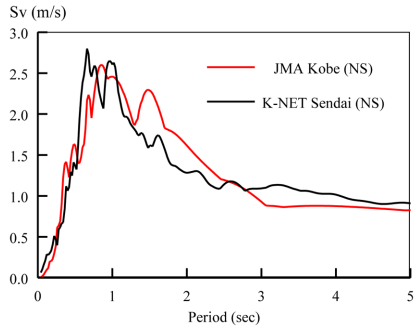

Figure 3. Pseudo velocity response spectrums (5% damping).

the K-Net Sendai was recorded at Sendai which is 176.5 km from the epicenter (K-Net SGM database). The duration of Kobe earthquake was about 30 seconds, however, the Tohoku earthquake lasted for at least 180 seconds. Pseudo velocity response spectrums with 5% damping were plotted in Fig. 3. The Kobe spectrum and the Tohoku spectrum are very similar to each other for all periods. It tells that structures and components are likely to be subjected to a small number of large amplitude loading cycles during near-fault earthquakes, when great amount of earthquake energy is inputted into the buildings in a short period of time. On the other hand, when the building is subjected to a long-duration earthquake, the energy is inputted into it throughout the whole duration. It this case, structures and structural components are subjected to a large number of loading cycles with small amplitudes.

Considering the safety of high-rise buildings with relatively longer nature period, it is necessary to evaluate the plastic deformation capacity of structural components and connections subjected to a number of cyclic loadings with small amplitudes. Researchers and designers in Japan have been discussing the influence of long-duration strong earthquake ground motions during the past decades. Most of them are experimental approaches to estimate the mechanical behavior of structural components and connections under many small amplitude loading cycles (Seki et al., 2012). Besides loading histories, there are other important parameters such as the material's yield strength/ratio, elongation, the beam's cross section, moment gradient. Experiment is one of the feasible methodology in evaluating the effects of these parameters on the beam's behavior. However, it is impossible and unpractical to cover all the parameters in real tests. Analytical approach which can take into account the material characteristics, the geometric features including the connection details, and random loading histories would be an effective method to evaluate the plastic deformation capacity of steel beam governed by the ductile fracture at the beam-end flange.

Among the existing evaluation method of the material damage, the one bases on the decomposition of the hysteresis loop of the steel was proved to be an accurate evaluation method in predicting steel fracture under large-amplitude strain histories in plastic region such as seismic effects (Jiao et al., 2010). In this evaluation method, the true stress-strain hysteresis loop of structural steel under random cyclic axial loadings was divided into three parts: the skeleton curve, Bauschinger part, and the elastic unloading part (Akiyama, 1985) as shown in Fig. 4, where the skeleton curve is obtained by connecting parts of the true stress-strain relation of both tension and compression sides sequentially, when the steel experienced its highest stress for the first time. Based on this methodology, a new attempt to evaluate a beam's plastic deformation capacity under long-duration earthquakes through numerical analysis is introduced in this paper. The above mentioned characteristics of steel beam-to-column connections were well simulated in the numerical analysis of beam-to-column connections, both site welded and shop welded

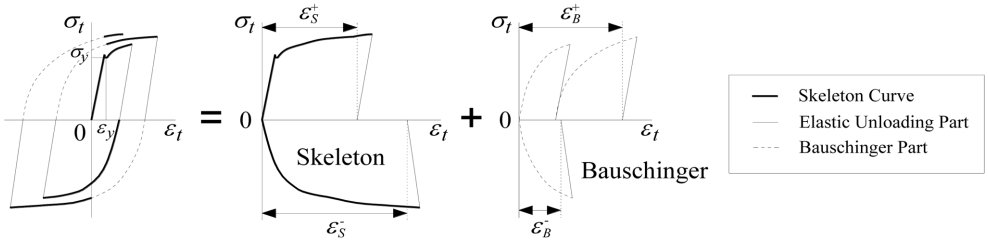

Figure 4. Decomposition of the stress-strain hysteresis loops.

types. The accuracy of this method was proved through experiments.

2. In-plane Analysis of Steel Beam-to-Column Connections

2.1. Basic assumption

The in-plane analysis of the ideal cantilever wide-flange beams subjected to cyclic loading histories was conducted under the following assumptions:

1) The assumption of the plane section.
2) The deformation due to shear force is considered to be always elastic.
3) There is no out-of-plane deformation of the beam.
4) The beam reaches its maximum load without local buckling.

2.2. Analytical algorithm

The algorithm of this analysis is based on the monotonic in-plane analyses in (Kato et al., 1966; Yamada et al., 1966; Yamada et al., 1995). The details of the analytical algorithm are illustrated in the appendix. The basic idea is to obtain the moment-curvature relation (*M-j*) of a certain beam section through the internal force balance under the assumption of the plane section. Additionally, the load-deformation relation (*M-q*) of the beam can be derived by integrating the moment-curvature relation along the beam span. This analytic method is known to be sufficiently accurate before the beam reaches its maximum strength. However, the decrease of the joint efficiency was not simulated in the analyses in Kato et al., 1966, Yamada et al., 1966, and Yamada et al., 1995.

2.3. Material hysteresis model

A material hysteresis model that is effective in material damage evaluation is very important for the cyclic beam analysis in this study. A multi-linear hysteresis model of structural steel considering Bauschinger effects based on the monotonic true stress-strain relation (Yamada et al., 2002) (Fig. 5) was employed in this analysis. The hyste-

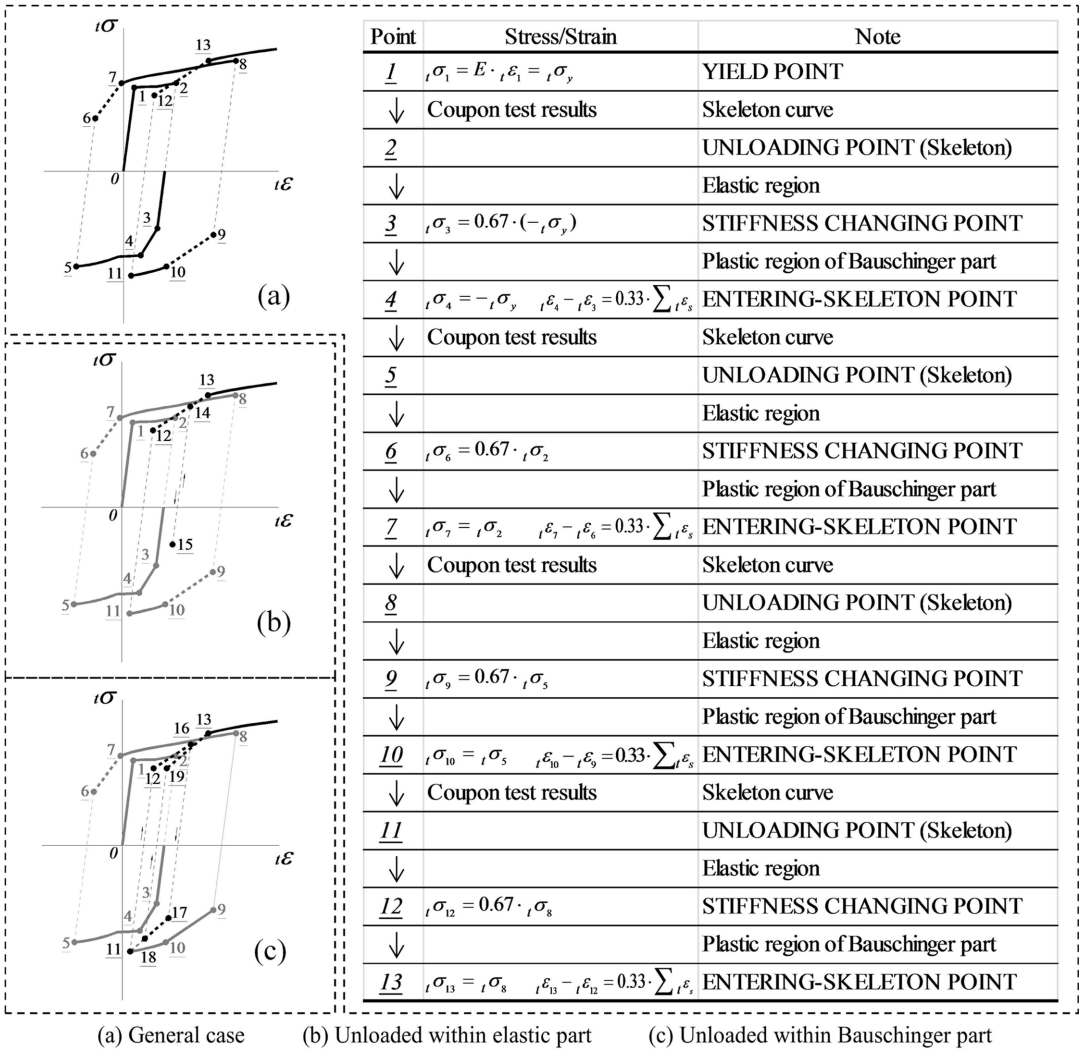

Point	Stress/Strain	Note
1	$_t\sigma_1 = E \cdot {}_t\varepsilon_1 = {}_t\sigma_y$	YIELD POINT
↓	Coupon test results	Skeleton curve
2		UNLOADING POINT (Skeleton)
↓		Elastic region
3	$_t\sigma_3 = 0.67 \cdot (-{}_t\sigma_y)$	STIFFNESS CHANGING POINT
↓		Plastic region of Bauschinger part
4	$_t\sigma_4 = -{}_t\sigma_y \quad {}_t\varepsilon_4 - {}_t\varepsilon_3 = 0.33 \cdot \sum {}_t\varepsilon_s$	ENTERING-SKELETON POINT
↓	Coupon test results	Skeleton curve
5		UNLOADING POINT (Skeleton)
↓		Elastic region
6	$_t\sigma_6 = 0.67 \cdot {}_t\sigma_2$	STIFFNESS CHANGING POINT
↓		Plastic region of Bauschinger part
7	$_t\sigma_7 = {}_t\sigma_2 \quad {}_t\varepsilon_7 - {}_t\varepsilon_6 = 0.33 \cdot \sum {}_t\varepsilon_s$	ENTERING-SKELETON POINT
↓	Coupon test results	Skeleton curve
8		UNLOADING POINT (Skeleton)
↓		Elastic region
9	$_t\sigma_9 = 0.67 \cdot {}_t\sigma_5$	STIFFNESS CHANGING POINT
↓		Plastic region of Bauschinger part
10	$_t\sigma_{10} = {}_t\sigma_5 \quad {}_t\varepsilon_{10} - {}_t\varepsilon_9 = 0.33 \cdot \sum {}_t\varepsilon_s$	ENTERING-SKELETON POINT
↓	Coupon test results	Skeleton curve
11		UNLOADING POINT (Skeleton)
↓		Elastic region
12	$_t\sigma_{12} = 0.67 \cdot {}_t\sigma_8$	STIFFNESS CHANGING POINT
↓		Plastic region of Bauschinger part
13	$_t\sigma_{13} = {}_t\sigma_8 \quad {}_t\varepsilon_{13} - {}_t\varepsilon_{12} = 0.33 \cdot \sum {}_t\varepsilon_s$	ENTERING-SKELETON POINT

(a) General case (b) Unloaded within elastic part (c) Unloaded within Bauschinger part

Figure 5. Multi-linear hysteresis model of structural steel considering Bauschinger effects (True stress-true strain relation).

resis loops are made up of the skeleton curves and the Bauschinger parts. The skeleton curves are picked up from the coupon tests results (converted into the true stress-strain relation). Each fragment of the Bauschinger part is simplified as a bi-linear curve, with the requirement that the bi-linear curve dissipates approximately same amount of plastic energy as the Bauschinger part does.

In this model, the entering skeleton point and the unloading point in the skeleton curve (unloading point (skeleton)) (Fig. 5) are reset every time if and only if the hysteresis loop enters its skeleton curve and remain unchanged until the hysteresis loop enters next skeleton curve fragment. Two basic rules are introduced (Eqs. (1)~(2)) in this hysteresis model. Fig. 3(a) shows an example of the hysteresis loops based on this model.

At each Entering-skeleton Point

$$\Delta_t\varepsilon = 0.33 \cdot \Sigma_t\varepsilon_S \tag{1}$$

At each Stiffness changing Point

$${}_t\sigma_{CS} = 0.67 \cdot {}_t\sigma_S \tag{2}$$

where $\Delta_t\varepsilon$ is the true strain increment from the "stiffness changing point" to the next "entering-skeleton point" (loops *3*-*4*, *6*-*7*, *9*-*10*, and *12*-*13* in Fig. 5(a)), and $\Sigma_t\varepsilon_S$ is the cumulative (true) skeleton strain till each "entering-skeleton point". In Eq. (2), ${}_t\sigma_{CS}$ is the true stress at the point when the hysteresis loop changes its stiffness from the elastic stiffness to the second stiffness due to the Bauschinger effect (point *3*, *6*, *9*, and *12* in Fig. 5(a)), and ${}_t\sigma_S$ is the true stress of the current unloading point (skeleton).

When unloading starts within the elastic region (point *15* in Fig. 5(b)), the loop will go back to the current unloading point (point *14* in Fig. 5(b)) in the plastic region and continue growing with the same slope (loop *15*-*14*-*13* in Fig. 5(b)).

Fig. 5(c) shows the case of unloading within the plastic region of Bauschinger part. Before unloading, the plastic region heads to the next entering skeleton point (loop *12*-*16* in Fig. 5(c), which heads to point *13*). At the stiffness changing point *17*, the true stress ${}_t\sigma_{17} = 0.67 \cdot {}_t\sigma_{11}$. The plastic region of Bauschinger part after the stiffness changing point (loop *17*-*18* in Fig. 5(c)) goes toward the unloading point in the skeleton curve (point *13* in Fig. 5(c)).

Note here, in the first cycle of the hysteresis loop, the true stress-strain curve on the compression side is also counted as skeleton curve because this is the first time for the material to experience highest/lowest stress, although Bauschinger effect is considered in this part (loop *3*-*4* in Fig. 5(a)).

In addition, the true stress-strain relation of the material is derived from the nominal stress-strain relation through Eqs. (3)~(4).

True strain:

$${}_t\varepsilon = \ln(1 + {}_n\varepsilon) \tag{3}$$

True stress:

$${}_t\sigma = {}_n\sigma(1 + {}_n\varepsilon) \tag{4}$$

where ${}_n\varepsilon$ is the nominal strain, and ${}_n\sigma$ is the nominal stress.

2.4. Modeling of the connection details

In the WF composite beam connected to RHS column that is commonly used in Japan, ductile fracture occurs mostly due to the decrease of the web's joint efficiency and the strain concentration on the bottom flange. The simulation of the connection details is a very important issue in the beam analysis. The loss of beam section due to the weld access holes and the local out-of-plane bending of the tube wall of the RHS column cause the strain concentration at the beam-end flange (Fig. 6), which directly leads to the early fracture (Matsumoto et al., 2002). The joint efficiency of the beam web at the connection is reduced (the beam-to-column connection's moment trans-

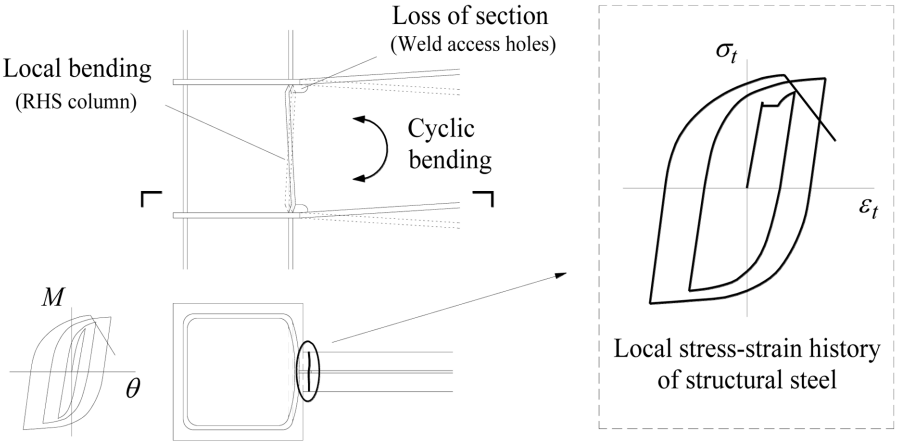

Figure 6. Decrease of the joint efficiency and the strain concentration at the beam-end flange.

mission capacity is less than 100%). To simulate this phenomenon, the analytical model of the in-plane beam analysis took into consideration the decrease of the joint efficiency.

The joint efficiency of the beam web at the beam-to-column connection γ_w is defined in Eq. (5) (Architectural Institute of Japan, 2006).

$$\gamma_w = \frac{{}_jM_{wu}}{M_{wu}} \tag{5}$$

where ${}_jM_{wu}$ is the maximum moment of the beam web at the connection considering the loss of the beam section and local bending of the column tube wall, $M_{wu} = \sigma_{wu} \cdot Z_{wp}$ is the ideal maximum moment of the beam web at the connection, σ_{wu} is the tensile strength of the beam web, and Z_{wp} is the plastic section modulus of the full section beam web. The calculation method of γ_w (Eq. (6)) is suggested in the Japanese "Recommendation for design of connections in steel structures" (Architectural Institute of Japan, 2006).

$${}_jM_{wu} = m \cdot Z_{wpe} \cdot \sigma_{wy} \tag{6}$$

where σ_{wy} is the yield stress of the beam web, Z_{wpe}=1/4 $(H - 2t_f - 2S_r)^2 \cdot t_w$ is the plastic section modulus of the beam web considering the loss of cross section, and m (Architectural Institute of Japan, 2006; Suita et al., 2000) is the normalized bending strength of the beam web at the beam-to-column connection $m = {}_jM_{wu}/M_{wp}$, where M_{wp} is the full plastic moment of the beam web considering the loss of section due to the weld access holes. Here, m is controlled by the size of the column, beam, and the weld access holes as well as the yield strengths of the column and beam. In design, it is possible to approximate m as follows: for the RHS columns, $m = \min\{1,\ 4(t_c/d_j)\sqrt{b_j \cdot \sigma_{cy}/t_w \cdot \sigma_{wy}}\}$, where σ_{cy} is the yield stress of the column, H is the beam height, t_f is the thickness of the beam flange, S_r is the loss of cross section in the beam height dimension (usually the length of the weld access hole along the beam height), t_w is the thickness of the beam web, t_c is the thickness of the RHS column, d_j is the inner distance of two diaphragms, $b_j = B_c - 2t_c$ is the width of the yield area on the RHS column obtained from the yield line theory, and B_c is the width of the RHS column. In this paper, only the most commonly used steel beams with weld access holes are discussed.

In the recent monotonic beam analysis (Suzuki et al., 1999), a part of the beam web (the isosceles right triangle ABC in Fig. 7) close to the column face was set to be ineffective in transferring the bending stress from the column. So that the ultimate moment (when the stress at each point of the web section equals to the ultimate strength of beam web σ_{wu}) of rest of the web cross section would be the same as ${}_jM_{wu}$ mentioned previously. h_r is the length of the ineffective area in the web along the beam height, which can be expressed in Eq. (7).

$$h_r = \sqrt{1 - \frac{m \cdot \sigma_{wy}}{\sigma_{wu}}} \cdot (H - 2 \cdot t_f - 2 \cdot S_r) \tag{7}$$

Nevertheless, this method didn't consider the loss of section due to weld access holes. With the effect of the weld access holes, the ineffective area of the web should be the pentagon ADCEB.

Furthermore, in case of shop welded connections, two rectangles at the location of the weld access holes, with the length of each side equals to S_r and the length of the weld access hole along the beam span respectively, should also be set to be ineffective in carrying the bending stress. Fig. 7(a) shows three ineffective parts of the beam close to the column face in the analysis. Note here, shear force is carried by the net beam section without weld access holes. On the other hand, for site welded connections, the bolts on the beam web start to slip when the beam section yields. The bending moment transmitted from the column face to the beam web is mainly through the bearing stress at the wall of the far-side bolt-holes. Hence, the web area surrounded by the column face, beam flange and the far-side bolt in Fig. 7(b), is set to be ineffective in carrying the bending stress.

Moreover, comparing with the beam flange, the strength

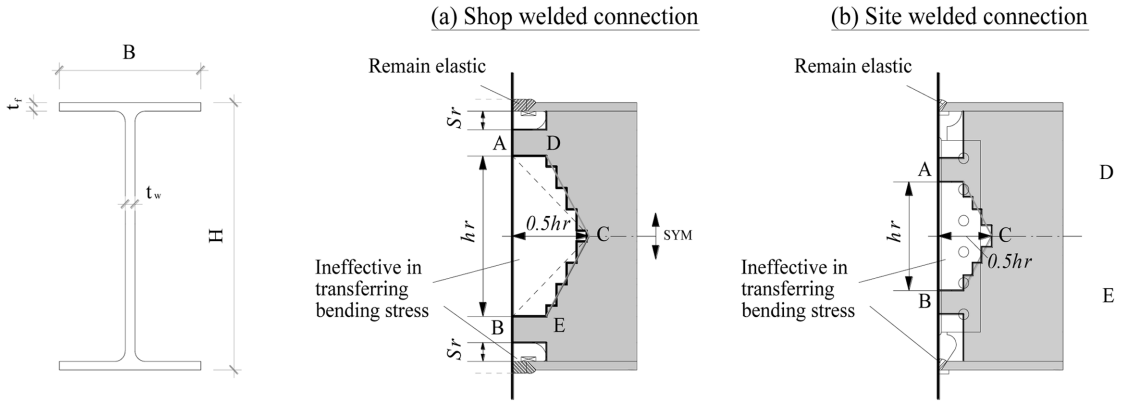

Figure 7. The ineffective area of the beam web.

of the diaphragms and the full-penetrated weld area is considered to be much higher. In the cyclic in-plane beam analysis, these parts were assumed to be always elastic (Fig. 6).

2.5. Mesh generation

The size of the meshes along the beam span is 10 mm, evenly. The mesh size changes along the beam height: The mesh density is larger at where the in-plane moment is larger. Both flanges are split into 5 meshes. The beam web within the height of each weld access hole is divided into 7 meshes. The rest of the web section is split into meshes with the size of 10~20 mm.

3. Verification of the Numerical Analysis

3.1. Basic information of the cyclic loading tests of steel beam-to-column subassemblies under small amplitude loading histories

In order to verify the analytical method introduced in Section 2, ten T-type beam-column subassemblies (Table 1) were tested under four different loading histories. Among them, three specimens initialed "K" were shop-welded specimens, while the others initialed "G" were site-welded specimens. The basic information of the specimens are listed in Table 1. Two types of beam sections were employed, with the beam depth of 600 mm or 800 mm. The column in each specimen has the same cross section of 500×500×25.

Fig. 8 shows the picture of the test setup and Fig. 9 shows the connections of both type of the specimens. The connection details were designed in accordance with the Japanese Standard Specification JASS 6 (Architectural Institute of Japan, 1996). Tensile coupon tests of both the beam (SM490) flange, web, and the column (SN490C) were performed using JIS-1A testing samples (Architectural Institute of Japan, 1996). The material characteristics are shown in Table 1 as well.

In order to investigate the beam's behavior during long-duration earthquakes, loading histories with small amplitudes were employed in these tests. For specimens tested under constant amplitude loadings, the number in each specimen's name indicates the loading amplitude in terms of the multiple of θ_P (from 0.9~3.0), the elastic beam

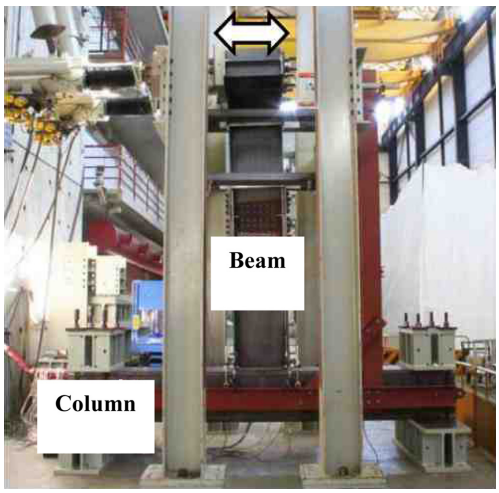

Figure 8. Test setup.

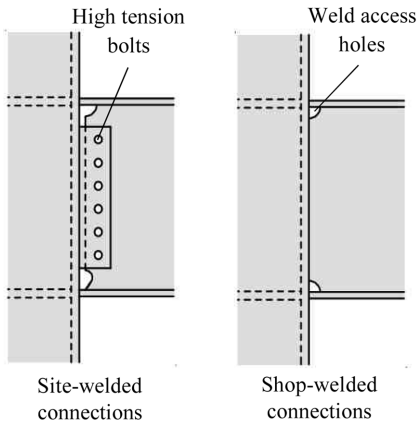

Figure 9. Two types of specimen connections.

Table 1. Basic information of the specimens

Name	Beam						Loading history	θ_{max}/θ_P	Connection type
	Cross section W-H×B×t_w×t_f	Span (mm)	Flange σ_y (N/mm^2)	Web σ_y (N/mm^2)	Cross section □-D×t_c	σ_y (N/mm^2)			
K-13	W-600×200×12×19	3000	337	364	□-500×25	370	Constant	1.3	Shop welded
K-20	W-600×200×12×19	3000			□-500×25		Constant	2	
K-30	W-600×200×12×19	3000			□-500×25		Constant	3	
G-13	W-600×200×12×19	3000	337	364	□-500×25	370	Constant	1.3	Site welded
G-20	W-600×200×12×19	3000			□-500×25		Constant	2	
G-30	W-600×200×12×19	3000			□-500×25		Constant	3	
G-R1	W-600×200×12×19	3000	337	364	□-500×25	370	Varying	2	
G-R2	W-600×200×12×19	3000			□-500×25		Varying	1.6	
GL-13	W-800×300×16×32	3000	357	372	□-500×25	355	Constant	1.3	
GL-20	W-800×300×16×32	3000			□-500×25		Constant	2	

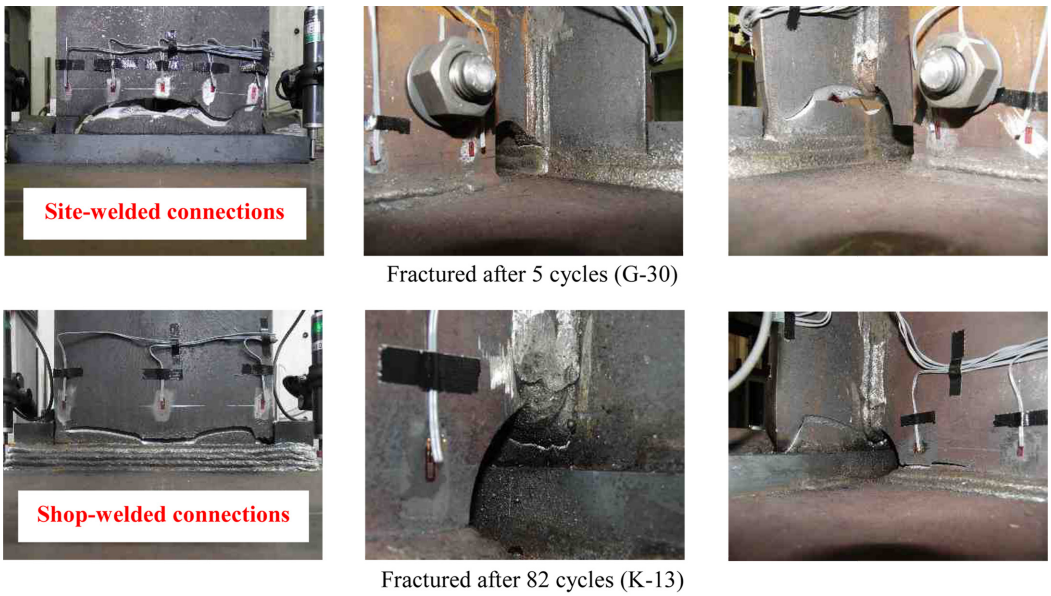

Figure 10. Examples of the ultimate situation of the specimens.

rotation when the moment of the beam's cantilever end equals its full plastic moment M_P. Specimen G-R1 was tested under varying-amplitudes loading from 0.8~2.0θ_P, while the loading amplitudes for specimen G-R2 was from 0.8~1.6θ_P.

All specimens ended in flange ductile facture during loading (Fig. 10). The number of loading cycles until fracture was larger when decreasing the loading amplitudes. The ultimate state of the specimen during the tests is defined as the point when the peak moment in a certain loading cycle drops below 90% of the maximum moment of the whole loading procedure.

The load-deformation relation and local strain history of the flange surface 50 mm from the column face (strain gauges' positions) were collected.

3.2. Comparison of the experimental and analytical results

3.2.1. Load-deformation relation

The in-plane analysis of all the steel beams specimens in the database was conducted. Fig. 11 shows the comparison of analytical and the experimental results of the load-deformation relations of some specimens. The results of two shop-welded specimens, three site-welded specimens tested under constant amplitude loading histories, two site-welded specimen tested under varying-amplitude loading history, and one site-welded specimen with its depth of 800 mm are shown in this figure. Good correspondences between the experimental and analytical results can be found from these graphs.

3.2.2. Strain history at beam-end flange

The measurements of the plastic strain gauges on each flange are compared with the nominal analytical strain history results at the same position, shown in Fig. 11. The experimental strain value of certain flange is the average value of the gauges attached on the flange.

For shop-welded connects, the analytical strain histories of the beam flange match the experimental strain histories well before fracture occurred. When it comes closer to the fracture points, although relatively larger disagreement can be seen from the graph, it is within the range of tolerable range. The disagreement observed might because of the soar of the local strain due to the sudden strain concentration at the fracture area on the flange. In addition, there is also a possibility of the existence of the measurement error from the plastic strain gauges after many loading cycles in large strain regions. For site-welded connections, because the local measuring data of the flange strain suddenly changed violently when the bolts slipped, it is hard to obtain the beam-end strain histories of the specimens. Therefore, the comparison of strain histories of site-welded connections is omitted in this paper.

Summing up the above verification, the cyclic in-plane beam analysis is effective in simulating the overall beam behavior (load-deformation relation) and local material behavior (strain history) during the loading procedure till fracture.

4. Evaluation of the Plastic Deformation Capacity of Steel Beams Based on the Strain Capacity of the Beam-End Flange

The essence of beam fracture lies in the fracture of the structural steel at the critical zone of the beam flange (Fig. 6). Thus the plastic strain capacity of the structural steel at the expected fracture zone of the beam is one of the key factors that determine the plastic deformation capa-

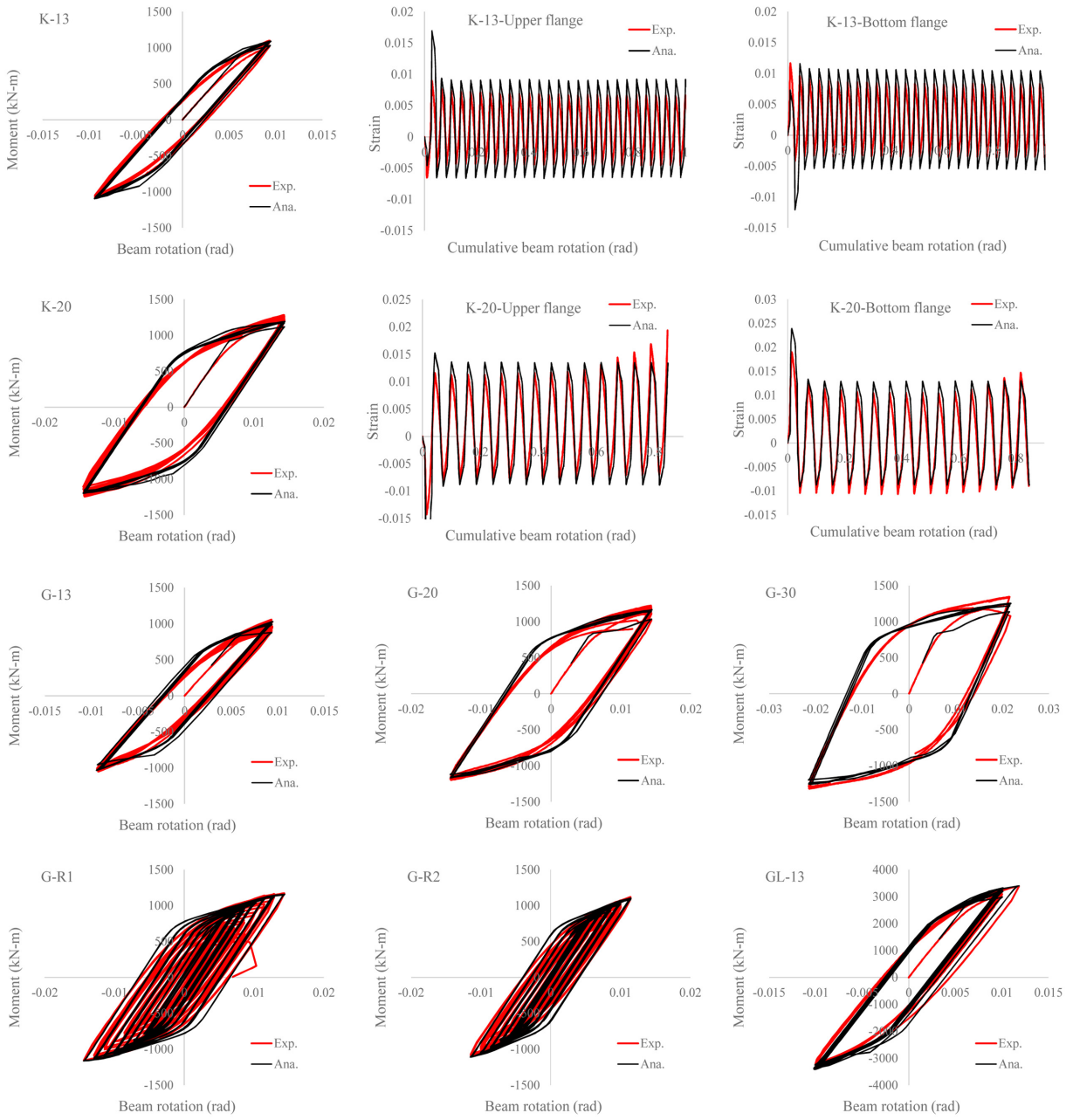

Figure 11. Comparison of the analytical and experimental results.

city of the beam. As mentioned previously, the true stress-strain hysteresis loop of structural steel under random cyclic axial loadings can be divided into three parts: the skeleton curve, Bauschinger part, and the elastic unloading part (Fig. 4). With the strain histories at the toe of the weld access holes obtained from the analysis, the plastic strain capacity of the beam-end flange was evaluated by study the relation between the strain capacities of each part of the hysteresis loop.

The cumulative plastic strain at the toe of the weld access holes of both tension and compression side in the skeleton curve and Bauschinger part is expressed as ($_t\varepsilon_S^+$, $_t\varepsilon_S^-$, $_t\varepsilon_B^+$ $_t\varepsilon_B^-$) respectively (Fig. 12). The ultimate total cumulative plastic strain is the summation of the value in each part ($_t\varepsilon_P$). Fig. 12 shows the relationship between the total cumulative plastic strain and the cumulative plastic strain in the skeleton curve during the loadings towards the tension direction when the specimen reached its ultimate state. Both $_t\varepsilon_S$ and $_t\varepsilon_P$ were divided by ε_0 (uniform elongation) in order to eliminate the influence of each different material. Here, uniform elongation is defined as the true strain obtained from the coupon test results, at the point when the engineering stress during reaches its peak value.

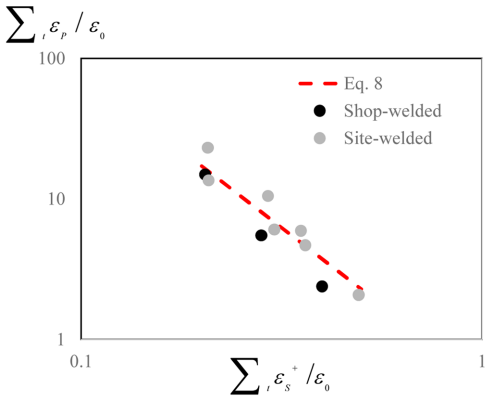

Figure 12. Relationship of cumulative strain in skeleton curve and the total plastic cumulative strain (at the beam-end flange).

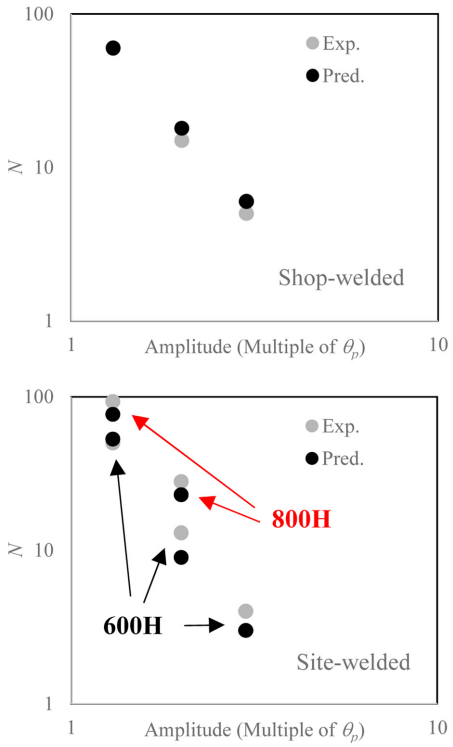

Figure 13. Comparison of the Experimental results and the predicted results on the number of loading cycles until ultimate states.

Fig. 12 shows the relationships between the normalized $\Sigma_t\varepsilon_S^+$ and $\Sigma_t\varepsilon_P$ of each specimens at their ultimate states. The results of shop-welded connection specimens are plotted in black circles and those of site-welded connections in gray circles. It can be found from Fig. 12 that the plots at the ultimate states of these specimens form an approximately linear relationship. Eq. (8) indicates the linear relationships between these two factors.

Eq. (8) is regarded as the fracture condition of steel beam-to-column connections under small amplitude cyclic loadings, using the evaluation method based on skeleton curve. This kind of loading histories corresponds with the seismic effect applied to the beams in high-rise buildings under long-duration earthquakes. In Fig. 13, the number of loading cycles until the beam's ultimate states obtained from the tests and the predicted number of loading cycles until failure are compared. For both shop-welded and site-welded connections, the predicted results show only small errors, especially for the beam-to-column connections under small amplitude loadings. In the group of site-welded connections, those beams with the depth of 800 mm results in large number of loading cycles than those with 600 mm mainly because the joint efficiency of the 800 mm is larger in this experiment. The evaluation method predicts the same trend, which confirms that the in-plane analysis manages to simulate the details of the beam-to-column connection as well as the effect of the joint efficiency.

5. Conclusions

The plastic deformation capacity of the structural components till ductile fracture plays a significant role in seismic design because it is one of the indexes of structural performance. High-rise buildings are extremely sensitive to long-duration earthquakes, when the structures and structural components are subjected to a large number of loading cycles with small amplitudes. Other than experimental method, this paper presents an evaluation method of plastic deformation capacity of steel beams in high-rise buildings under long-duration earthquakes, based on a numerical in-plane analysis.

The fracture condition of the steel beam flange was discussed by studying the average flange surface stress-strain history of the beam section at the toe of the weld access hole. The in-plane analyses of the steel beams subjected to small amplitude cyclic loading histories were conducted to obtain the above mentioned average stress-strain history. A hysteresis model of the structural steel considering Bauschinger effect, which is effective in evaluating material damage, was introduced into this analysis. Moreover, the analytical model takes into account the decrease of the joint efficiency, which directly affects the strain capacity of the beam flange.

The analytical load-deformation relation as well as the local strain histories are compared to the experimental results, good correspondences have been found between the results. The analytical simulation was proved to be authentic. Meanwhile, the analytical evaluation method was also confirmed to be able to predict the failure number of loading cycles with small error. Given all that, the proposed evaluation method is effective in evaluating the plastic deformation capacity of steel beam-to-column connections in moment resisting frames under long-duration earthquakes.

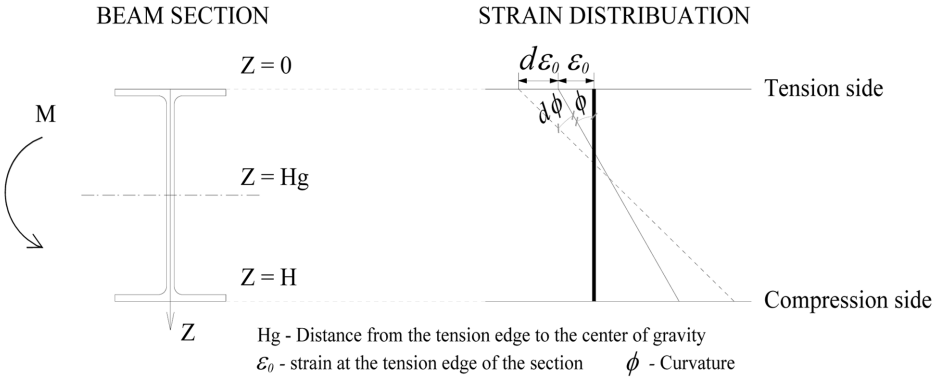

Figure A1. Internal force balance of the beam section.

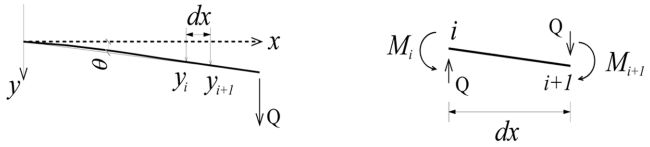

Figure A2. Mesh generation along the beam span.

APPENDIX

Calculation of the moment-curvature relation

The moment-curvature relation of a certain section was obtained by the internal force balance in the beam section. Fig. A1 shows the internal force balance of the beam section. The width of the beam section is the function of the distance from the section tension edge $g(Z)$. The stress value at each point in this section is the function of the strain value at that point $f(\varepsilon)$. Therefore, the axial force P and bending moment M can be written as:

$$P=\int_0^H f(\varepsilon)\cdot g(Z)dz=\int_0^H f(\varepsilon_0+\phi\cdot Z)\cdot g(Z)dz \tag{A1}$$

$$\begin{aligned} M&=\int_0^H f(\varepsilon)\cdot g(Z)\cdot Zdz-P\cdot Hg \\ &=\int_0^H f(\varepsilon_0+\phi\cdot Z)\cdot g(Z)\cdot Zdz-P\cdot Hg \end{aligned} \tag{A2}$$

by given the section a small curvature increment $d\phi$, Eqs. (A1) and (A2) change to:

$$P+dP=\int_0^H f(\varepsilon_0+d\varepsilon_0+(\phi+d\phi)\cdot Z)\cdot g(Z)dz \tag{A3}$$

$$\begin{aligned} &M+dM \\ &=\int_0^H f(\varepsilon_0+d\varepsilon_0+(\phi+d\phi)\cdot Z)\cdot g(Z)\cdot Zdz-P\cdot Hg \end{aligned} \tag{A4}$$

where $d\varepsilon_0$ is the increment of tension edge strain. In this study, the steel beams were subjected to pure bending, therefore, $P = 0$, $dP = 0$. Eqs. (A3) and (A4) were derived using Taylor expansion. Here terms after the 2nd term are considered negligible. Through Eqs. (A5) and (A6), it is able to obtain the moment curvature relation.

$$d\varepsilon_0=\frac{\int_0^H f'(\varepsilon_0+\phi\cdot Z)\cdot g(Z)\cdot ZdZ}{\int_0^H f'(\varepsilon_0+\phi\cdot Z)\cdot g(Z)dZ}\cdot d\phi \tag{A5}$$

$$dM=\int_0^H f'(\varepsilon_0+\phi\cdot Z)\cdot(d\varepsilon_0+d\phi\cdot Z)\cdot g(Z)\cdot Zdz \tag{A6}$$

Calculation of the moment-rotation relation

The moment-rotation relation of the beam was derived by integrating the moment-curvature relation along the beam span. The beam was divided into meshes with the size of 10 mm. In a certain mesh No i [i, i+1], the boundary condition is shown in Fig. A2. The curvature of a certain mesh is considered to be constant. Therefore,

$$y''=\phi_i \tag{A7}$$

$$\theta=y'=\phi_i\cdot x+C_1 \tag{A8}$$

$$y=0.5\cdot\phi_i\cdot x^2+C_1\cdot x+C_2 \tag{A9}$$

for mesh No i, suppose the boundary condition θ_i and y_i are known, then,

$$\theta_{i+1}=\theta_i+\phi_i\cdot\Delta x \tag{A10}$$

$$y_{i+1}=y_i+\theta\cdot\Delta x+0.5\cdot\phi_i\cdot\Delta x^2+\frac{Q\cdot\Delta x}{G\cdot A_w} \tag{A11}$$

where G is the shear stiffness, and A_w is the area of the

beam web. Furthermore, from the force balance in mesh No i, the moment of i+1 point can be obtained by Eq. (A12).

$$M_{i+1} = M_i - Q \cdot \Delta x \quad \text{(A12)}$$

References

Architectural Institute of Japan. (1996). "Japanese architectural standard specification JASS 6," Steel work. Tokyo: AIJ. (In Japanese).

Architectural Institute of Japan. (2006). "Recommendation for design of connections in steel structures." Tokyo: AIJ. (In Japanese).

Akiyama, H. (1985). "Earthquake-resistant limit-state design for buildings," Tokyo: University of Tokyo Press.

Building Research Institute and the Japan Iron and Steel Federation. (2002). "Study on testing method for structural performance evaluation of steel structures." Tokyo.

Clark, P., Frank, K., Krawinkler, H., and Shaw, R. (1997). "Protocol for fabrication, inspection, testing, and documentation of beam-column connection tests and other experimental specimens." SAC Steel Project Background Document, Report No. SAC/BD-97/02.

Jiao, Y., Yamada, S., and Kishiki, S. (2010). "Plastic deformation capacity of structural steel under various axial strain histories." 8th International Conference on Urban Earthquake Engineering. Tokyo, Japan, pp. 935~940.

Kato, B., Akiyama, H., and Uchida, N. (1966). "Ultimate strength of structural steel members (I)." Transactions of the AIJ; No 119, pp. 22~30. (In Japanese).

Matsumoto, Y., Yamada, S., and Akiyama, H. (2000). "Fracture of beam-to-column connections simulated by means of the shaking table test using the inertial loading equipment." Behaviour of Steel Structures in Seismic Areas, Balkema, Rotterdam, pp. 215~222.

Nakashima, M., Inoue, K., and Tada, M. (1998). "Classification of damage to steel buildings observed in the 1995 Hyogoken-Nanbu earthquake." *Eng. Struct.*, 20(4-6), pp. 271~281.

Roeder, C. W. (2002). "Connection performance for seismic design of steel moment frames." *Journal of Structural Engineering*, 128(4), pp. 420~428.

Seki, K., Narihara, H., Yasuda, S., and Hasegawa, T. (2012). "Study on Safety Assessment Methods for Super-high-rise Steel Buildings against Long-period Earthquake Ground Motions (Part II): Multi-cycle Loading Test of Welded Beam-to-Column Connection (Outline of Test)." Proceedings of the AIJ Annual Meeting, Nagoya. (in Japanese).

Suita, K. and Tanaka, T. (2000). "Flexural strength of beam web to square tube column joints." *Steel Construction Engineering*, 7(26), pp. 51~58. (in Japanese).

Suzuki, T., Ishii, T., Morita, K., and Takanashi, K. (1999). "Experimental study on fracture behavior of welded beam-to-column joint with defects." *Steel Construction Engineering*, 6(23), pp. 149~164. (In Japanese).

Yamada, M., Sakae, K., Tadokoro, T., and Shirakawa, K. (1966). "Elasto-plastic bending deformation of wide flange beam-columns under axial compression, Part I: Bending moment-curvature and bending moment-deflection relations under static loading." *Journal of Structural and Construction Engineering*, Transactions of the AIJ; 127, pp. 8~14. (In Japanese).

Yamada, S. and Akiyama, H. (1995). "Deteriorating behavior of steel members in post-buckling range." *Structural Stability and Design*, Balkema, Rotterdam, pp. 169~174.

Yamada, S., Imaeda, T., and Okada, K. (2002). "Simple hysteresis model of structural steel considering the Bauschinger effect" (In Japanese). *Journal of Structural and Construction Engineering*. Transactions of AIJ; No 559, pp. 225~232.

Youssef, N., Bonowitz, D., and Gross, J. L. (1995) "A survey of steel moment-resisting frame buildings affected by the 1994 Northridge earthquake." NISTIR 5625, National Institute of Standards and Technology.